

Mineralogical characterization of clay mineral assemblages from Rio de Janeiro pegmatites to identify kaolinite and/or halloysite deposits

(Caracterização mineralógica das associações de argilominerais em pegmatitos do estado do Rio de Janeiro com enfoque na identificação de depósitos de caulinita e/ou halloysita)

V. M. J. Salgado-Campos^{1,2*}, L. C. Bertolino^{2,3}, F. J. da Silva⁴, J. C. Mendes¹

¹Federal University of Rio de Janeiro, Institute of Geosciences, Graduate Program in Geology, Av. Athos da Silveira Ramos 274, 21941-909, Rio de Janeiro, RJ, Brazil

²Center for Mineral Technology, Division for Mineral Analyses, Sector for Mineral Technology, Rio de Janeiro, RJ, Brazil

³State University of Rio de Janeiro, Faculty of Geology, Department of Mineralogy and Igneous Petrology, Rio de Janeiro, RJ, Brazil

⁴Federal Rural University of Rio de Janeiro, Institute of Agronomy, Department of Petrology and Geotectonic, Seropédica, RJ, Brazil

Abstract

This study reports the mineralogical characterization of kaolin occurrences in the State of Rio de Janeiro, Brazil, to identify new kaolinite and halloysite deposits. Samples were collected in 10 pegmatites with varying sizes for X-ray diffractometry, chemical analysis by X-ray fluorescence, and scanning electron microscopy studies. The results indicated that the kaolin occurrences were of weathered origin, wherein some places there were occurrences of tubular halloysite. Concerning the regolith stratigraphy, samples located in the saprock zone were found to contain kaolinite and/or halloysite contents from 0 to 10.1%, while those located in the saprolite zone contained kaolinite and/or halloysite contents from 16.3% to 34.9%. Kaolinite and/or halloysite-7Å were formed from plagioclase weathering instead of K-feldspar or mica, and the halloysite-7Å occurrence was related to samples in regions with a higher degree of weathering.

Keywords: kaolin, kaolinite, halloysite, Rietveld, Rio de Janeiro.

Resumo

Este estudo reporta a caracterização mineralógica de ocorrências de caulim no estado do Rio de Janeiro, Brasil, com enfoque na identificação de depósitos de caulinita e/ou halloysita. Amostras foram coletadas em 10 pegmatitos de dimensões variadas para estudos de difratometria de raios X, análise química por fluorescência de raios X e microscopia eletrônica de varredura. As ocorrências de caulim nos corpos pegmatíticos foram de origem intempélica, onde em alguns locais houve ocorrência de halloysita tubular. Dentro da estratigrafia do regolito, as amostras localizadas na zona de saprock apresentaram teores de caulinita e/ou halloysita entre 0 e 10,1%, enquanto aquelas localizadas no saprólito apresentaram maiores teores de caulinita entre 16,3% e 34,9%. A caulinita e/ou halloysita foram formadas a partir da alteração de plagioclásio e não de K-feldspato ou mica, estando a ocorrência de halloysita associada a locais de grau de intemperismo mais elevado.


Palavras-chave: caulim, caulinita, halloysita, Rietveld, Rio de Janeiro.

INTRODUCTION

Kaolin is a fine-grained white rock/ore composed mostly of kaolinite, halloysite, or other kaolinite polytypes [1]. The material is used in many industrial segments, mainly in the ceramic and paper industries [2]. Moreover, halloysite kaolin deposits have been studied since 2005 [3] for nobler

applications in nanotechnology because the substance is considered to be a more environmentally friendly nanotube source [4]. It is used in pharmaceuticals as an active principle carrier [5], in polymers as filler [6], as well as to make anticorrosive paint [7], among others. Kaolin deposits can be classified as primary when arising from *in situ* silicate alteration, typically of feldspar, or as secondary, when having sedimentary origin [8]. There are primary kaolin deposits hosted in pegmatites, which are generally granitic rocks with coarser grain size than the host rock [9], and that can be zoned or not [10]. These lithologies are found in pegmatite

*victorsalgadocampos@hotmail.com

 <https://orcid.org/0000-0001-7662-1186>

provinces, which are large areas containing a considerable number of pegmatite bodies. This type of deposit can have a hydrothermal or weathering origin, in the last case where the quality is associated with the pegmatite weathering degree. Concerning regolith stratigraphy, kaolin deposits generally occur in the saprolite zone, which has a higher weathering degree, while deposits in the saprock zone, which are located between the crude rock and saprolite zones, have lesser kaolinite and/or halloysite contents. Saprock forms the zone where less than 20% of weatherable minerals are weathered, while saprolite is in the zone where more than 20% of the weatherable minerals are weathered [11].

Besides Brazil, kaolinitic kaolin deposits are found in the Hagendorf-Pleystein Pegmatite Province (Germany) [12] and the Spruce Pine deposit (USA) [13], while kaolinite and halloysite mixtures are found in the Bombowha deposit (Ethiopia) [14, 15] and the Swat deposits (Pakistan) [16]. Brazil is the world's 7th-leading kaolin producer, with 1.7 Mtpa [17], and its deposits are found mainly in the Capim River [18] and Jari River [19] sedimentary deposits in the North region, and in the primary deposits of the Borborema Pegmatite Province [20-22] and Oriental Pegmatite Province [23, 24]. In the Brazilian Southeast and South regions, kaolin deposits from the Oriental Pegmatite Province are found in the State of Minas Gerais, primary deposits hosted in granites in São Paulo [25], primary deposits hosted in acid volcanic rocks in Paraná [26] and Santa Catarina [27], and primary deposits hosted in anorthosites in the Rio Grande do Sul [25]. There is also a small kaolin occurrence in Espírito Santo [28]. In Rio de Janeiro State, nowadays, there are kaolin occurrences in the municipalities of Magé [24], Valença [24], Sapucaia [29], Petrópolis [29], Itatiaia [30], Araruama [30], and Rio de Janeiro [31], while other kaolin deposits in the State's northern region were depleted between 1940 and 1980 [32]. Data concerning kaolin production in Rio de Janeiro is quite inaccurate, as well as data about the volume and estimated reserves. Generally, the kaolin production in Rio de Janeiro is made by small companies, which do not have conditions to size ore reserves with precision. Studies to identify prospective new occurrences in the Rio de Janeiro, as well as its mineralogical description is necessary to understand the mining potential of the State, where dozens of pegmatite bodies are cataloged [33] but have not been studied to detect kaolin. Therefore, here we report the mineralogical, chemical, micromorphological, and genetic characterization of kaolin occurrences in Rio de Janeiro to identify new commercial deposits.

MATERIALS AND METHODS

Sampling sites: the overall study area was the Rio de Janeiro Pegmatite Province, Brazil, which was subdivided into 5 areas: Niterói-Rio Bonito; Cantagalo-São Fidélis; Paraíba do Sul; Casemiro de Abreu-Glicério; and Barra Mansa-Barra do Pirai (Fig. 1) [32]. The first two were visited for the prospection of pegmatite bodies, in which the catalog of pegmatites from Rio de Janeiro [33] was used as a guide to investigating the pegmatites

described as having kaolin occurrences. The Cantagalo-São Fidélis area, containing the municipality of Cantagalo, covers 3300 km² and has the occurrence of pegmatites named Córrego do Ouro (CA-3), Esmério (CA-4), and Boa Sorte Superior (CA-2), the first two with kaolin occurrences. The Niterói-Rio Bonito area, covering the municipalities of Rio Bonito, São Gonçalo, and Maricá, has 1700 km² and contains the pegmatite bodies designated RB-1, RB-2, RB-3, RB-4, RB-5, RB-6, RB-7, SG-1, SG-2, SG-3, SG-4, and Calaboca-Rebentão, in which bodies SG-2, SG-3, SG-4, and Calaboca-Rebentão did not present kaolin occurrences. In Cantagalo, the Córrego do Ouro pegmatite body has a length of 25 m and a height of nearly 15 m, from which feldspar was extracted in the 1980s (Fig. 2A). The Esmério pegmatite body, probably the biggest in Rio de Janeiro, has a length of 200 m, the height of 50 m, with lenticular geometry, and was utilized to mine feldspar and rubellite during the 1960s, where kaolin occurrences were also identified (Figs. 2B and 2C). The Boa Sorte Superior pegmatite body was exploited for mica and kaolin during the 1940s, by open-pit mining, which was reactivated in 1970 to extract feldspar. The pegmatite body there is 30 m high and 8 m wide, with no occurrence of kaolin [33]. In Rio Bonito, the RB-1 pegmatite occurs on a road cut and has large dimensions (Fig. 2D). The RB-2 pegmatite apparently was already exploited and is nearly 10 m long and 8 m wide (Fig. 2E). The RB-3 pegmatite is 5 m in length, width, and height and is reddish (Fig. 2F). The RB-4 pegmatite deposit has many small pegmatite bodies with a centimeter thickness (Figs. 2G and 2H) with kaolin occurrence. The RB-5 pegmatite is 10 m high, 4 m long, and 2 m wide (Fig. 2I). The RB-6 pegmatite is 10 m long and 10 m high, where there is white-colored kaolin occurrence (Fig. 2J). The RB-7 pegmatite can be associated with alkaline rocks and has small dimensions (Fig. 2K). In São Gonçalo, the SG-1 pegmatite deposit is located in a quarry, with an approximate thickness of 3 m and is discordant, wherein the uppermost portion contains kaolin (Fig. 2L). The SG-2, SG-3, and SG-4 bodies do not present kaolin occurrences, nor does the Calaboca-Rebentão pegmatite (MA-1).

16 samples from the 10 pegmatite bodies previously described were collected (Table I). The samples were dried at 60 °C for 24 h, submitted to jaw crushing to produce <2 mm grain size and divided into aliquots of 1 kg. Then, smaller aliquots were submitted to vibratory ring milling for 30 s at 700 rpm to obtain fractions less than 106 µm with precautions to avoid sample amorphization. After that, the fractions were processed in a McCrone mill to generate fractions less than 10 µm for quantitative mineral analysis. Other aliquots of 1 kg were submitted to granulometric classification in wet conditions in vibratory sieves of 20 µm before the separation of the clay fraction using Stokes' law, employing an ultrasonic bath and sodium hexametaphosphate (3 mg/g) as dispersant agent. After that, bulk samples were analyzed by X-ray diffractometry (XRD) for quantitative mineral analysis and X-ray fluorescence spectroscopy (XRF) for chemical analysis. Clay size fractions were studied through XRD and scanning electron microscopy (SEM). X-ray diffractograms for quantitative mineral analysis were acquired in a Bruker D4 Endeavor diffractometer with

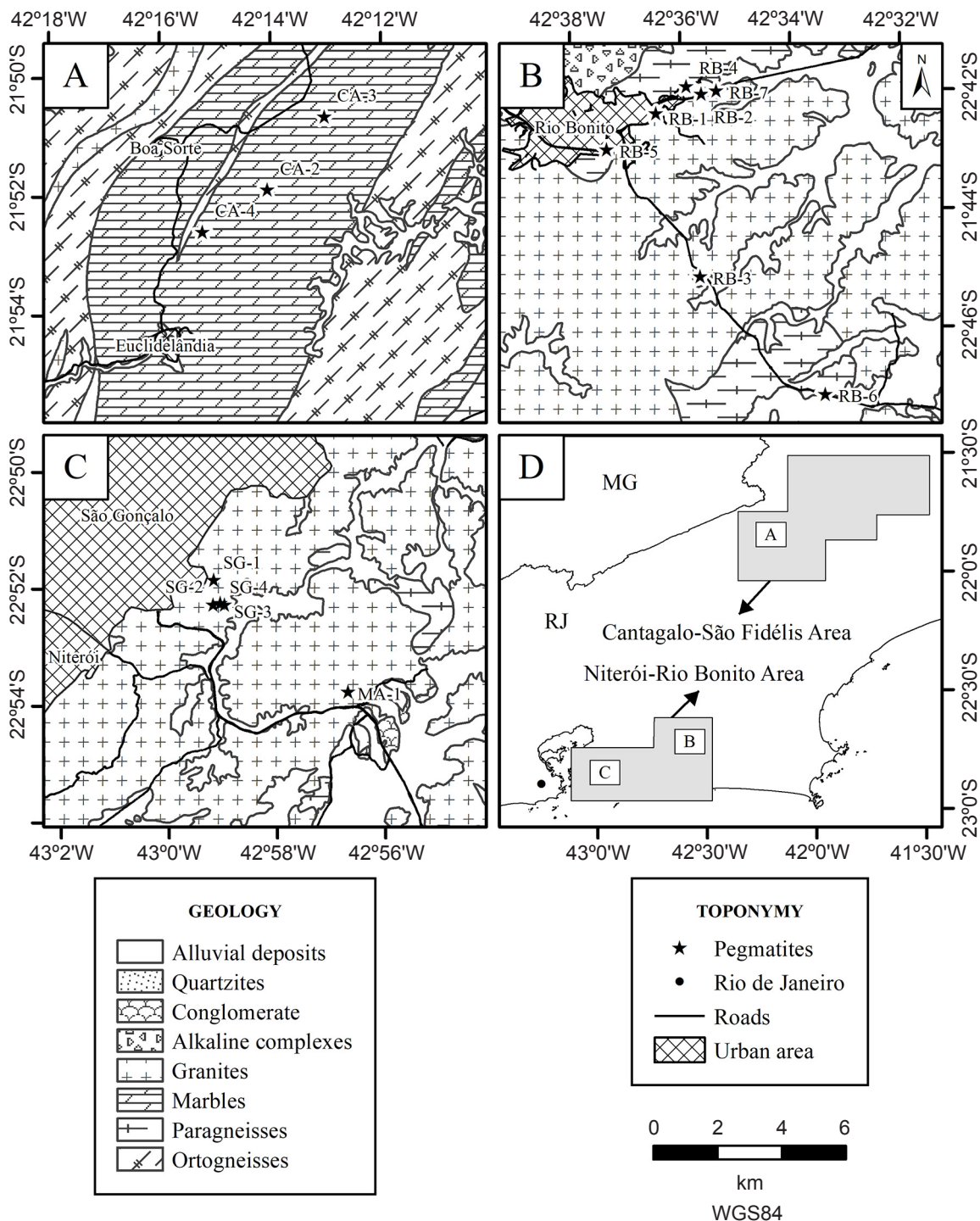


Figure 1: Geological map with sampling locations in the Rio de Janeiro Pegmatite Province (RJPP), in which the scale bar is associated with maps A, B, and C [32, 34]: A) Cantagalo-São Fidélis area; B) site near Rio Bonito in the Niterói-Rio Bonito area; C) site near São Gonçalo in the Niterói-Rio Bonito area; and D) map of the central portion of Rio de Janeiro State, highlighting the Cantagalo-São Fidélis and Niterói-Rio Bonito areas in the geological context of the RJPP, containing the locations of maps A, B, and C.

[Figura 1: Mapa geológico com localizações de coleta das amostras na Província Pegmatítica do Rio de Janeiro (PPRJ), onde a escala está associada aos mapas A, B e C [32, 34]: A) área Cantagalo-São Fidélis; B) área próxima a Rio Bonito na área Niterói-Rio Bonito; C) área próxima a São Gonçalo na área Niterói-Rio Bonito; e D) mapa da porção central do estado do Rio de Janeiro com destaque para as áreas Cantagalo-São Fidélis e Niterói-Rio Bonito no contexto geológico da PPRJ, onde estão assinaladas as localidades dos mapas A, B e C.]

CoK α ($\lambda=1.79021$ Å) radiation, operated at 40 kV and 40 mA with goniometer velocity of 0.01° (2θ) per 1 s in the range between 4° and 105° (2θ). The quantitative mineral

analysis was performed with software (TOPAS v.5, Bruker), and structures available in the ICDD database (2019) were used in the refinement [35]. Sample positions in regolith

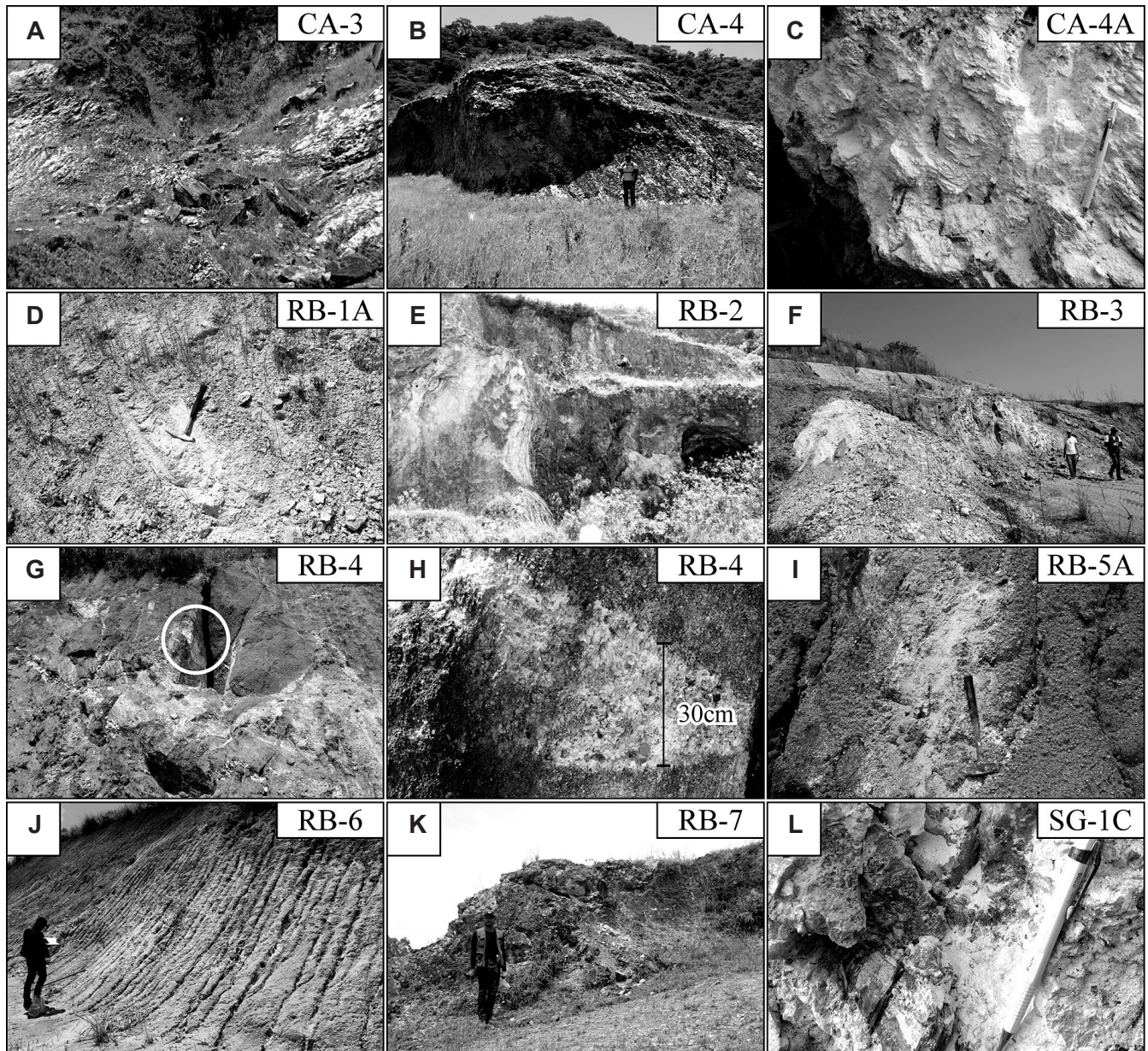


Figure 2: Pegmatite body images: A) Córrego do Ouro (CA-3) front view; B) feldspar mining front view from the 1960s in the Esmério pegmatite (CA-4); C) sampling location of kaolin (CA-4A) in the Esmério pegmatite; D) RB-1 pegmatite; E) front view of RB-2 pegmatite; F) side view of body RB-3; G) overview of the pegmatite swarm in RB-4; H) detailed view (circle in 2G), in which the sampling took place; I) sampling location of RB-5A; J) side view of RB-6 pegmatite; K) body RB-7; and L) sampling location in SG-1 pegmatite.

[Figura 2: Imagens dos pegmatitos: A) visão frontal do pegmatito Córrego do Ouro (CA-3); B) frente de lavra de feldspato da década de 1960 no pegmatito Esmério (CA-4); C) local de amostragem de caulim (CA-4A) no pegmatito Esmério; D) pegmatito RB-1; E) vista frontal do pegmatito RB-2; F) visão lateral do corpo RB-3; G) visão afastada do enxame de pegmatitos no ponto RB-4; H) região em detalhe (círculo em 2G), onde foi realizada a amostragem; I) local de coleta da amostra RB-5A; J) visão lateral do pegmatito RB-6; K) corpo RB-7; e L) local de amostragem no pegmatito SG-1.]

stratigraphy (RE) were verified through Eq. A, in which $Kln+Hly$ is the sum of the kaolinite and halloysite contents, Sm is the smectite content, Kfs is the K-feldspar content, Pl is the plagioclase content, and $Mi+Ill$ is the sum of mica and illite contents (since the differentiation of mica and illite is not possible through XRD). When the result is $\leq 20\%$, the sample is from the saprock zone, while when the result is $>20\%$, the sample is from the saprolite zone [11].

$$RE = \frac{(Kln+Hly)+Sm}{Kfs + pl + (Mi+Ill) + (Kln+Hly)+Sm} \cdot 100 \quad (A)$$

Clay size fractions were analyzed through the oriented-slide method [36], in which samples on glass slides were air-dried, treated with ethylene-glycol for 16 h, and heated at 550 °C for 2 h. Then, X-ray diffractograms were acquired in the same diffractometer but using a goniometer velocity

Table I - Sampling sites in the Cantagalo-São Fidélis and Niterói-Rio Bonito areas.
 [Tabela I - Locais de amostragem nas áreas Cantagalo-São Fidélis e Niterói-Rio Bonito.]

Pegmatite	Number of samples	Area	Municipality	Latitude	Longitude	Elevation (m)
Córrego do Ouro (CA-3)	2	Cantagalo-São Fidélis	Cantagalo	-21.842	-42.217	332
Boa Sorte Superior (CA-2)	0*	Cantagalo-São Fidélis	Cantagalo	-21.863	-42.233	370
Esmério (CA-4)	2	Cantagalo-São Fidélis	Cantagalo	-21.875	-42.251	426
RB-1	2	Niterói-Rio Bonito	Rio Bonito	-22.708	-42.607	74
RB-2	2	Niterói-Rio Bonito	Rio Bonito	-22.703	-42.593	71
RB-3	2	Niterói-Rio Bonito	Rio Bonito	-22.754	-42.593	97
RB-4	1	Niterói-Rio Bonito	Rio Bonito	-22.700	-42.598	74
RB-5	2	Niterói-Rio Bonito	Rio Bonito	-22.719	-42.622	75
RB-6	1	Niterói-Rio Bonito	Rio Bonito	-22.786	-42.554	71
RB-7	1	Niterói-Rio Bonito	Rio Bonito	-22.702	-42.589	59
Calaboca-Rebentão (MA-1)	0*	Niterói-Rio Bonito	Maricá	-22.895	-42.946	41
SG-1	1	Niterói-Rio Bonito	São Gonçalo	-22.863	-42.987	63
SG-2	0*	Niterói-Rio Bonito	São Gonçalo	-22.863	-42.987	76
SG-3	0*	Niterói-Rio Bonito	São Gonçalo	-22.870	-42.987	96
SG-4	0*	Niterói-Rio Bonito	São Gonçalo	-22.870	-42.984	85

* no occurrence of kaolin.

of 0.01° (2θ) per 0.5 s in the range between 2° and 40° (2θ). The diffractograms used for distinguishing clay minerals species using $d(060)$ reflections [37] were obtained with random mounted samples in the interval between 1.84 and 1.46 Å in a diffractometer (D8 Advance, Bruker) with $\text{CuK}\alpha$ ($\lambda=1.5406$ Å) radiation in the conditions of 40 kV and 25 mA, goniometer velocity of 0.02° (2θ) per step with a counting time of 0.5 s per step. The quantification of clay minerals was made following the Biscaye's method [38], in which the area of the main basal reflection of each clay mineral (d_{001}) in the diffractograms obtained from the ethylene-glycol solvated glass slides was measured in relation to the sum of all peak areas, being weights attributed to them in order to correct the effect of full width at half-maximum of each clay mineral. The method states that smectite, illite, and kaolinite receive weights 1, 4, and 2, respectively, and, in the present study, rectorite received weight 1.

Chemical analysis was carried out by X-ray fluorescence spectroscopy (XRF) in a spectrometer (Axios mAX, PANalytical) in which the fractions were prepared in an automatic press (Vaneox) with 20 mm diameter with a pressure of 20 ton for 30 s, utilizing boric acid (H_3BO_3 , Merck, R.G.) in the proportion of 1:0.1. The loss on ignition (LOI) was quantified in duplicate through the difference between the sample mass before and after heating at 1000°C for 16 h. The quantitative mineral analysis values were converted into chemical analysis values and compared to the

XRF results, considering the chemical compositions of the minerals from an open-source website (www.webmineral.com), except kaolinite and halloysite which oxide contents were based on unpublished data (Table II). The chemical analysis was also used to obtain the chemical index of alteration (CIA) [39] through Eq. B, in which the oxides' molar proportions were used, considering only CaO content

Table II - Chemical compositions (wt%) used in the conversion of results from quantitative mineral analysis to chemical analysis.

[Tabela II - Composições químicas (% em massa) usadas na conversão dos resultados de análise mineral quantitativa em análise química.]

Content	Mo	Ms	Kln/Hly	Qtz	Kfs	Pl
SiO_2	43.77	45.21	43.22	100.00	64.76	67.39
Al_2O_3	18.57	38.36	42.82	0.00	18.32	20.35
CaO	1.02	0.00	0.00	0.00	0.00	1.07
Na_2O	1.13	0.00	0.00	0.00	0.00	11.19
K_2O	0.00	11.81	0.00	0.00	16.92	0.00
LOI	36.09	4.07	13.96	0.00	0.00	0.00
F	0.00	0.55	0.00	0.00	0.00	0.00
Sum	100.58	100.00	100.00	100.00	100.00	100.00

Mo: montmorillonite; Ms: muscovite; Kln/Hly: kaolinite and/or halloysite; Qtz: quartz; Kfs: K-feldspar; Pl: plagioclase.

from silicate origin. The index was used to determine the weathering degree that rock was submitted.

$$CIA = \frac{Al_2O_3}{Al_2O_3 + CaO + Na_2O + K_2O} \cdot 100 \quad (B)$$

Pearson correlation coefficients (ρ), used to construct matrices, were calculated with the OriginPro2020 software, and the values obtained were classified following the convention in Table III. The scanning electron microscopy (SEM) images were acquired in a microscope (TM3030Plus, Hitachi) operating at 15 kV in a low vacuum mode. The samples were sputter-coated with silver in a sputter coater (SCD 005, Bal-Tec) for 250 s at 30 mA.

Table III - Classification by Pearson correlation coefficients. [Tabela III - Convenção utilizada para avaliação dos coeficientes de correlação de Pearson.]

ρ value (+ or -)	Interpretation
0.00 to 0.19	Very weak correlation
0.20 to 0.39	Weak correlation
0.40 to 0.69	Moderate correlation
0.70 to 0.89	Strong correlation
0.90 to 1.00	Very strong correlation

RESULTS

Quantitative mineral analysis (XRD) and chemical analysis (XRF): smectite was identified in samples CA-3B, RB-3B, and RB-5A by basal reflection at 15 Å (001), mica and/or illite were identified in all the samples by basal reflections at 9.98 Å (001) and 4.98 Å (002), kaolinite and/or halloysite in all the samples except CA-3 and RB-3B by basal reflection at 7 Å (001), quartz in all the samples by reflections at 4.25 Å, K-feldspar in all of the samples except RB-2, RB-3B, and RB-7 by reflections at 6.34 and 3.24 Å, and plagioclase in samples CA-3, CA-4, RB-1, RB-3A, and SG-1C by reflection at 3.18 Å (Fig. 3). In the Cantagalo area, kaolinite did not occur in the Córrego do Ouro pegmatite (CA-3), while two samples from Esmério pegmatite had contents close to 4% (Table IV). In Rio Bonito, RB-1 pegmatite showed kaolinite contents between 1.6% (RB-1B) and 6.4% (RB-1A), and RB-2 pegmatite presented kaolinite contents between 6.6% (RB-2B) and 16.3% (RB-2A). The RB-3 pegmatite contained kaolinite only in the sample RB-3B with 1.7%, while the RB-4 pegmatite had the greatest content, 34.9%. In the samples of RB-5 pegmatite, kaolinite contents between 17.2% (RB-5B) and 18.5% (RB-5A) were detected, while in RB-6 pegmatite, the kaolinite content was 23.9%. The RB-7 pegmatite contained the 2nd greatest kaolinite content, 33.3%. Last, the SG-1C pegmatite had a kaolinite content of 10.1%. Based on the regolith stratigraphy (RE) index, the samples CA-3, CA-4, RB-1, RB-2B, RB-

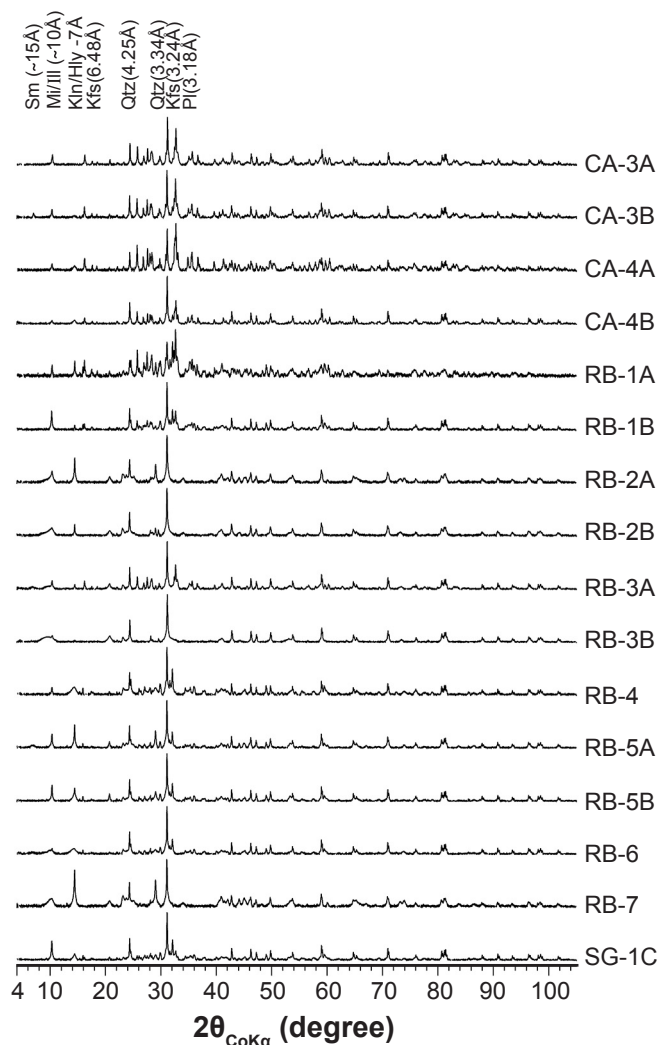


Figure 3: Normalized X-ray diffractograms of the bulk fractions separated by location (y-axis in quadratic scale). Sm: smectite; Mi: mica; Il: illite; Kln: kaolinite; Hly: halloysite; Qtz: quartz; Kfs: K-feldspar; Pl: plagioclase.

[Figura 3: Difratogramas de raios X das frações brutas separados por localidade (eixo y em escala quadrática). Sm: esmectita; Mi: mica; Il: illita; Kln: caulinita; Hly: halloysita; Qtz: quartzo; Kfs: K-feldspato; Pl: plagioclásio.]

3, and SG-1C came from the saprock zone, while samples RB-2A, RB-4, RB-5, RB-6, and RB-7 originated in the saprolite zone, which was where the greatest kaolinite and/or halloysite contents were found, between 16.3% and 34.9%. Through the correlation between the results of chemical analysis obtained from quantitative mineral analysis and XRF, it was possible to evaluate the refinement quality (Fig. 4). The Pearson correlation coefficient values ranged from 0.993 (RB-5A) to 1.000 (RB-1B), and the coefficient of determination (R^2) values ranged from 0.985 (RB-5A) to 0.999 (RB-1B).

Clay mineral assemblages: the mixture between kaolinite and/or halloysite and other clay minerals decreases the ore quality because beneficiation plants are unable to separate them. Therefore, clay mineral assemblages were determined

Table IV - Results of quantitative mineral analysis of the bulk fractions obtained by the Rietveld method and its figures of merit and chemical analysis by XRF in oxides and calculated indexes.

[Tabela IV - Resultados de análise mineral quantitativa das frações brutas através do método de Rietveld e suas figuras de mérito, e análise química por FRX em óxidos e índices calculados.]

	CA-3A	CA-3B	CA-4A	CA-4B	RB-1A	RB-1B	RB-2A	RB-2B	RB-3A	RB-3B	RB-4	RB-5A	RB-5B	RB-6	RB-7	SG-1C
Mineralogy (wt%)																
Sm	0.0	0.1	0.0	0.0	0.0	0.0	0.0	0.0	0.0	3.1	0.0	7.2	0.0	0.0	0.0	0.0
Mi+Ill	4.5	3.1	1.0	4.5	3.9	13.0	45.3	46.2	8.5	46.9	1.5	7.7	9.5	22.9	41.4	16.0
Kln+Hly	0.0	0.0	4.0	4.5	6.4	1.6	16.3	6.6	1.7	0.0	34.9	18.5	17.2	23.9	33.3	10.1
Qtz	31.9	27.8	13.6	44.8	9.2	35.5	38.4	47.2	31.8	50.0	27.1	44.3	48.5	36.4	25.4	43.3
Kfs	2.6	7.1	1.2	6.0	20.8	23.9	0.0	0.0	2.8	0.0	36.6	22.3	24.8	16.8	0.0	24.7
Pl	60.9	61.9	80.2	40.0	59.7	26.0	0.0	0.0	55.3	0.0	0.0	0.0	0.0	0.0	0.0	5.8
Sum	99.9	100.0	100.0	99.8	100.0	100.0	100.0	100.0	100.1	100.0	100.1	100.0	100.0	100.0	100.1	99.9
Rietveld (wt%)																
SiO ₂	76.7	75.6	70.6	79.8	67.4	75.1	66.1	71.1	75.4	72.7	66.5	73.4	76.3	68.0	58.6	74.9
Al ₂ O ₃	14.6	15.1	18.6	12.9	20.2	15.4	24.4	20.6	15.7	18.6	22.2	16.3	15.6	22.1	30.2	16.2
CaO	0.7	0.7	0.9	0.4	0.7	0.3	0.0	0.0	0.6	0.0	0.0	0.1	0.0	0.0	0.0	0.1
Na ₂ O	6.8	6.9	9.0	4.5	6.7	2.9	0.0	0.0	6.2	0.0	0.0	0.1	0.0	0.0	0.0	0.7
K ₂ O	1.0	1.6	0.3	1.6	4.0	5.6	5.4	5.5	1.5	5.6	6.4	4.7	5.3	5.6	4.9	6.1
LOI	0.2	0.2	0.6	0.8	1.1	0.8	4.1	2.8	0.6	3.0	4.9	5.5	2.8	4.3	6.3	2.1
Sum	99.99	100.0	100.0	100.0	100.0	100.0	100.0	100.0	100.0	100.0	100.0	100.0	100.0	100.0	100.0	100.0
Chemistry (wt%)																
SiO ₂	70.80	69.70	63.80	75.10	64.50	73.60	60.40	70.80	72.30	71.20	63.00	67.40	70.90	67.70	57.00	71.50
Al ₂ O ₃	18.20	18.70	24.10	16.60	22.20	15.60	26.40	16.00	17.30	18.10	25.90	23.30	20.50	21.90	30.10	19.40
Fe ₂ O ₃	0.47	0.60	0.27	0.26	0.74	1.00	2.60	3.30	0.46	1.60	0.48	0.68	0.80	1.00	1.10	0.91
MnO	0.00	0.00	0.00	0.00	0.00	0.00	0.15	0.05	0.00	0.00	0.00	0.00	0.00	0.00	0.00	0.00
MgO	0.17	0.15	0.00	0.00	0.27	0.50	0.46	0.81	0.56	0.83	0.28	0.40	0.17	0.58	0.53	0.24
CaO	1.40	1.50	2.50	1.40	0.15	0.51	0.00	0.00	0.27	0.05	0.00	0.00	0.00	0.00	0.00	0.20
Na ₂ O	7.10	7.30	7.40	4.20	6.20	3.20	0.00	0.00	4.50	0.19	0.31	0.17	0.22	0.23	0.00	1.10
K ₂ O	1.00	1.20	0.51	1.10	3.40	4.10	2.20	2.30	1.40	2.60	4.70	2.60	4.00	2.70	2.00	3.50
TiO ₂	0.00	0.00	0.00	0.00	0.05	0.15	0.15	0.83	0.05	0.51	0.00	0.19	0.05	0.10	0.43	0.00
P ₂ O ₅	0.00	0.00	0.00	0.00	0.11	0.05	0.11	0.05	0.00	0.00	0.00	0.00	0.00	0.00	0.00	0.00
ZrO ₂	0.00	0.00	0.00	0.00	0.00	0.00	0.13	0.05	0.00	0.00	0.00	0.00	0.00	0.00	0.17	0.00
LOI	0.65	0.74	1.20	1.20	2.40	1.20	7.20	6.00	3.20	5.10	5.40	5.20	3.40	5.70	8.80	2.80
Sum	99.79	99.89	99.78	99.86	100.02	99.91	99.80	100.19	100.04	100.18	100.07	99.94	100.04	99.91	100.13	99.65
Index																
CIA	54.32	53.84	58.25	60.93	61.07	59.48	91.73	86.54	64.77	84.91	82.23	88.28	81.38	86.90	93.29	76.49
RE	0.0	0.1	4.6	8.2	7.0	2.5	26.5	12.5	2.5	6.2	47.8	46.1	33.4	37.6	44.6	17.8
Parameter																
q	0.998	0.998	0.994	0.998	0.999	1.000	0.995	0.995	0.999	0.999	0.997	0.993	0.997	0.999	0.998	0.998
R ²	0.995	0.995	0.988	0.996	0.998	0.999	0.990	0.990	0.997	0.997	0.994	0.985	0.993	0.998	0.996	0.996
Figure of merit*																
GOF	2.32	2.44	2.23	1.96	2.06	2.20	2.63	2.62	2.31	2.95	2.44	3.07	2.33	2.13	3.82	2.85
R _{exp}	4.55	4.32	4.83	4.78	4.59	4.47	3.68	3.56	4.44	4.13	4.73	4.31	4.41	4.22	4.02	4.41
R _{wp}	10.57	10.55	10.75	9.36	9.44	9.82	9.67	9.34	10.27	12.19	11.56	13.24	10.25	9.01	15.36	12.54

Sm: smectite; Mi+Ill: mica+illite; Ill: illite; Kln+Hly: kaolinite+hallowite; Qtz: quartz; Kfs: K-feldspar; Pl: plagioclase; LOI: loss on ignition; CIA: chemical index of alteration; RE: regolith stratigraphy; q: Pearson correlation coefficient; R²: coefficient of determination; * evaluates the quality of the Rietveld refinement (the lower the value, the better the refinement); GOF: goodness of fit; R_{exp}: expected R-value; R_{wp}: weighted-profile R-value.

(Fig. 5). Despite the identification of smectite in the clay size fraction diffractograms, the small contents of the mineral caused difficulties in bulk fractions' quantification, since

smectite's main reflections in XRD, close to 15 Å (001), are only well-identified when reasonable quantities of the mineral are present. Smectite was identified in samples CA-

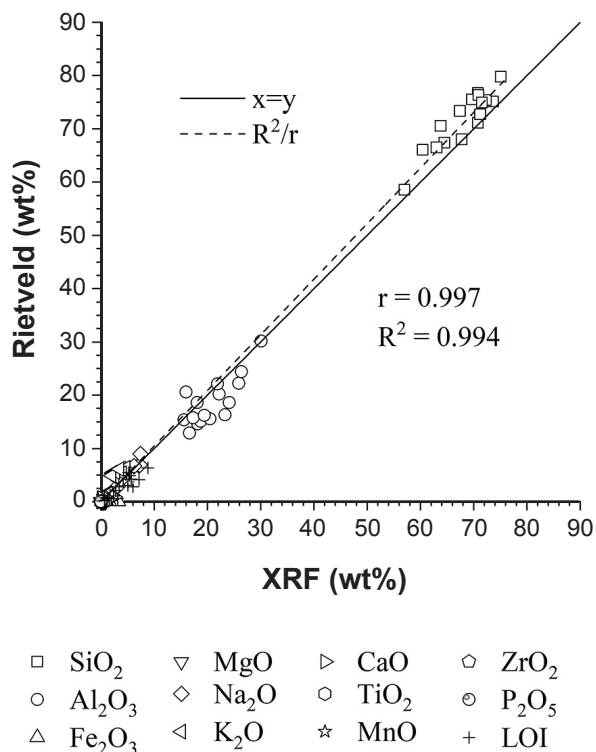


Figure 4: Correlation between the chemical compositions obtained from the conversion of the quantitative mineral analysis and X-ray fluorescence spectroscopy to evaluate the Rietveld refinement quality. The Pearson correlation coefficient and the R^2 value shown are related to all data.

[Figura 4: Correlação entre as composições químicas obtidas pela conversão da análise mineral quantitativa e espectroscopia de fluorescência de raios X visando avaliar a qualidade dos refinamentos por Rietveld. O coeficiente de correlação de Pearson e o valor de R^2 apresentados estão relacionados a todos os dados.]

3, RB-1, RB-3, RB-5, RB-6, and SG-1C by reflections at 15 Å, which expanded to 17 Å after treatment with ethylene glycol and collapsed after heating at 550 °C. Illite was identified in all the samples by reflections at 10 Å, which did not change after ethylene glycol treatment and heating at 550 °C. Kaolinite was identified in all the samples by reflections at 7 Å, which did not undergo changes after ethylene glycol treatment and collapsed after heating at 550 °C. Rectorite, an interstratified clay mineral between mica and smectite [40], was found in samples RB-2A and RB-3B by reflection at 24 Å, which expanded to 26.5 Å after ethylene glycol treatment. Through d(060) reflections, it was possible to identify clay mineral species. Montmorillonite was determined as the smectite group clay mineral because of reflections at 1.50 Å, which is also associated with illite, while kaolinite and/or halloysite were identified by reflections at 1.49 Å [37].

In the quantitative analysis of the clay mineral phases (Table V), the samples CA-3A and CA-3B were found to be mostly composed of montmorillonite, with concentrations of 67% and 47%, followed by kaolinite with values of 10% and 31% and illite with values of 24% and 22%, respectively. The samples CA-4A and CA-4B were almost entirely composed of kaolinite, with contents of 77% and

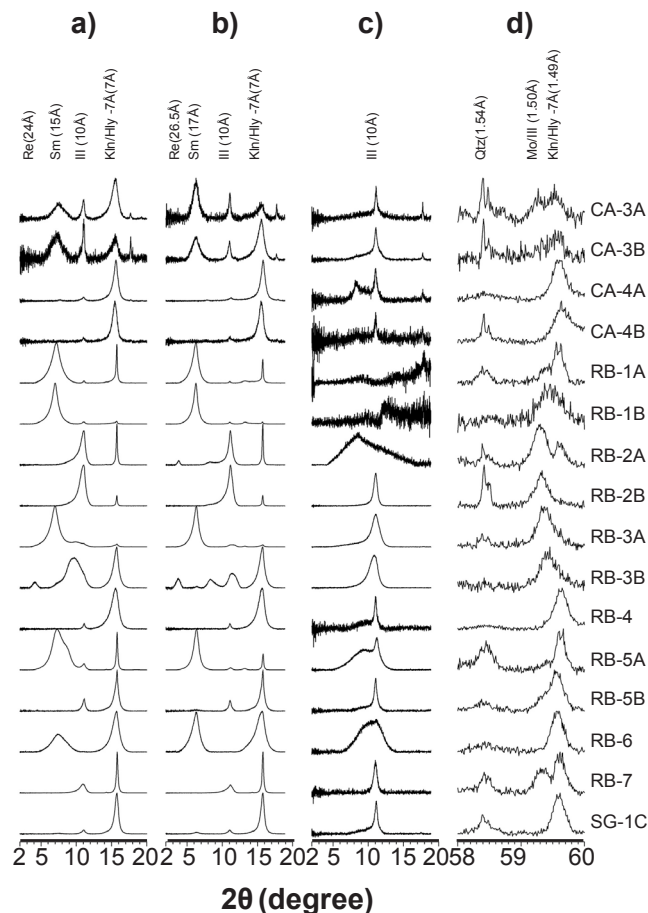


Figure 5: Normalized X-ray diffractograms of the clay size fractions prepared by air drying (a), solvated with ethylene glycol (b), and heated at 550 °C (c) on oriented slides and with random mounted fractions in the region between 1.84 and 1.46 Å for the investigations of d(060) reflections (d) to determine the species of clay minerals. Re: rectorite; Sm: smectite; Mo: montmorillonite; Ill: illite; Kln: kaolinite; Hly: halloysite; Qtz: quartz. Radiation: $\text{CoK}\alpha$ (a,b,c); $\text{CuK}\alpha$ (d).

[Figura 5: Difratogramas de raios X normalizados das frações de argila preparadas como lâminas orientadas secas ao ar (a), solvatadas com etilenoglicol (b) e aquecidas a 550 °C (c) e com montagem randômica na região entre 1,84 e 1,46 Å para investigação das reflexões de d(060) (d) para determinação dos argilominerais. Re: rectorita; Sm: esmectita; Mo: montmorillonite; Ill: illita; Kln: caulinita; Hly: halloysita, Qtz: quartz. quartz. Radiação: $\text{CoK}\alpha$ (a,b,c); $\text{CuK}\alpha$ (d).]

82%, and illite had values of 23% and 17%, respectively. Samples RB-1A and RB-1B were found to be composed of montmorillonite with contents of 91% and 94%, kaolinite with values of 7% and 3%, and illite with values of 1% and 3%, respectively. Samples RB-2A and RB-2B were composed mostly of illite, with concentrations of 86% and 99%, and in lesser proportions by kaolinite, with values of 6% and 1%, respectively. In sample RB-2A, rectorite was observed, with a content of 7%. Sample RB-3A was composed of 93% montmorillonite, 6% illite, and 1% kaolinite, while sample RB-3B presented 60% illite, 20% rectorite, 19% kaolinite, and 1% montmorillonite. Sample

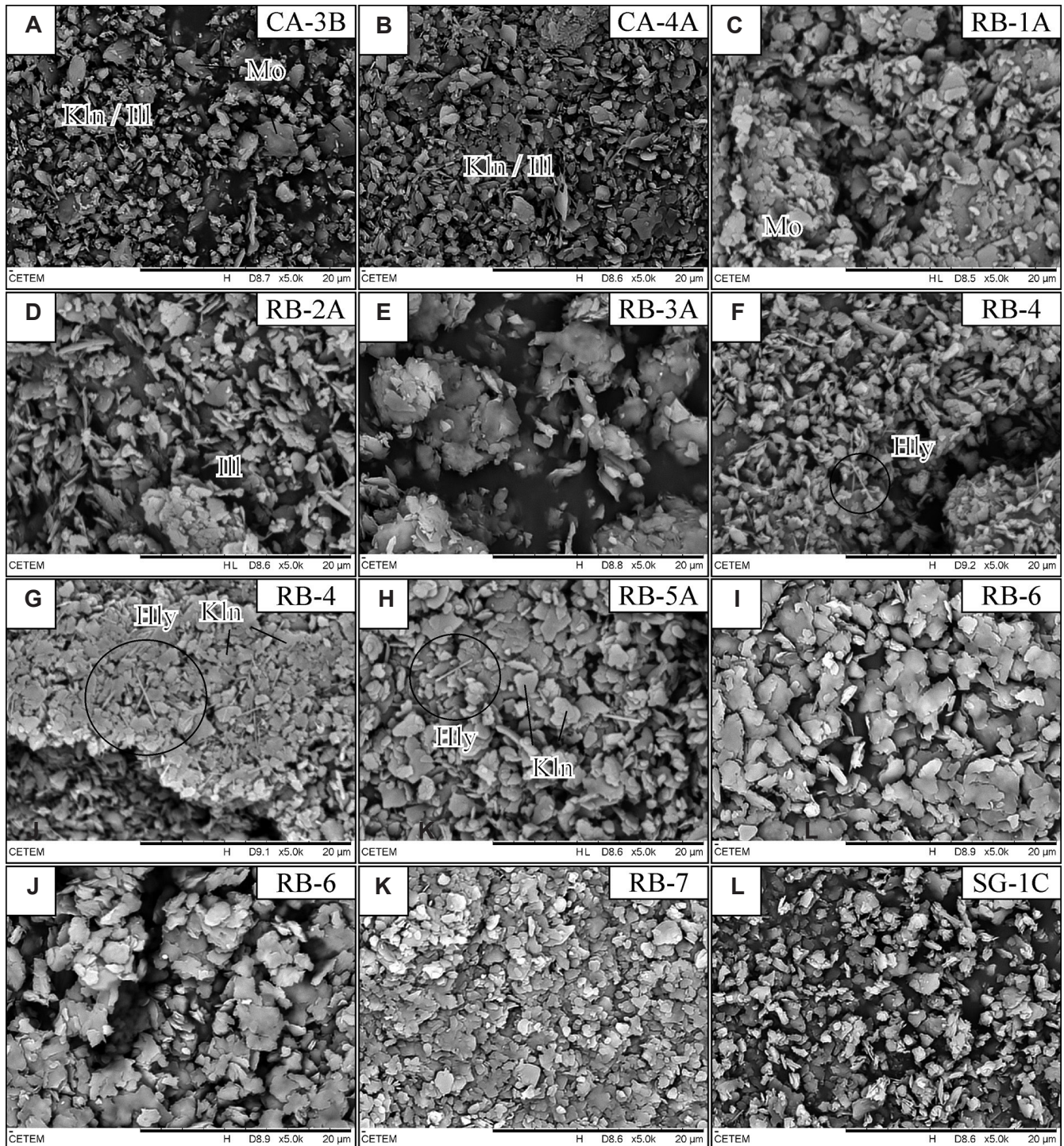


Figure 6: SEM images of clay size fractions: A) montmorillonite, illite, and kaolinite in fraction CA-3B; B) kaolinite and illite in fraction CA-4A; C) montmorillonite in fraction RB-1A; D) illite in fraction RB-2A; E) montmorillonite in fraction RB-3A; F,G) kaolinite and tubular halloysite in fraction RB-4; H) kaolinite and tubular halloysite in fraction RB-5A; I,J) kaolinite and montmorillonite in fraction RB-6; K) kaolinite and illite in fraction RB-7; and L) kaolinite and illite in fraction SG-1C.

[Figura 6: Imagens de microscopia eletrônica de varredura das frações de argila: A) montmorillonita, illita e caulinita na fração CA-3B; B) caulinita e illita na fração CA-4A; C) montmorillonita na fração RB-1A; D) illita na fração RB-2A; E) montmorillonita na fração RB-3A; F,G) caulinita e halloysita tubular na fração RB-4; H) caulinita e halloysita tubular na fração RB-5A; I,J) caulinita e montmorillonita na fração RB-6; K) caulinita e illita na fração RB-7; e L) caulinita e illita na fração SG-1C.]

because sedimentary deposits tend to be almost completely composed of kaolinite and/or halloysite. Concerning to the Campo Alegre deposits, which are more similar to the kaolin

occurrences from Rio de Janeiro, the contents of kaolinite and/or halloysite are close to values found in the Oxford mine (Ox1), indicating that the contents of kaolinite and/

Table VI - Pearson correlation matrix between the chemical index of alteration (CIA) and the results of quantitative mineral and chemical analyses.

[Tabela VI - Matriz de correlação de Pearson entre o índice químico de alteração (CIA) e resultados de análises mineral quantitativa e química.]

	CIA	Sm	Mi+Ill	Kln+Hly	Qtz	Kfs	Pl	Fs	SiO ₂	Al ₂ O ₃	Fe ₂ O ₃	MnO	MgO	CaO	Na ₂ O	K ₂ O	TiO ₂	P ₂ O ₅	ZrO ₂	LOI	
CIA																					
Sm	0.32																				
Mi+Ill	0.70	0.04																			
Kln+Hly	0.70	0.05	0.16																		
Qtz	0.45	0.34	0.42	-0.05																	
Kfs	0.05	0.11	-0.49	0.40	-0.01																
Pl	-0.91	-0.29	-0.62	-0.63	-0.65	-0.28															
Fs	-0.92	-0.30	-0.83	-0.49	-0.68	0.12	0.92														
SiO ₂	-0.45	0.03	-0.26	-0.67	0.53	0.07	0.17	0.20													
Al ₂ O ₃	0.51	0.07	0.15	0.78	-0.42	0.07	-0.26	-0.24	-0.95												
Fe ₂ O ₃	0.57	-0.03	0.85	0.03	0.40	-0.35	-0.53	-0.68	-0.14	-0.03											
MnO	0.39	-0.12	0.56	0.08	0.17	-0.34	-0.28	-0.42	-0.35	0.24	0.72										
MgO	0.59	0.22	0.78	0.09	0.37	-0.23	-0.56	-0.67	-0.03	-0.09	0.69	0.24									
CaO	-0.76	-0.22	-0.51	-0.51	-0.39	-0.34	0.81	0.70	0.16	-0.19	-0.47	-0.22	-0.67								
Na ₂ O	-0.94	-0.29	-0.64	-0.64	-0.62	-0.23	0.98	0.93	0.20	-0.29	-0.53	-0.30	-0.59	0.82							
K ₂ O	0.37	0.04	0.02	0.45	0.17	0.83	-0.60	-0.27	-0.03	0.09	0.11	-0.06	0.22	-0.69	-0.56						
TiO ₂	0.54	0.19	0.81	0.04	0.38	-0.41	-0.49	-0.67	-0.07	-0.07	0.79	0.24	0.79	-0.41	-0.51	0.02					
P ₂ O ₅	0.05	-0.19	0.28	-0.10	-0.25	-0.04	0.00	-0.01	-0.28	0.10	0.52	0.66	0.18	-0.26	0.00	0.21	0.15				
ZrO ₂	0.55	-0.15	0.67	0.46	-0.05	-0.44	-0.37	-0.55	-0.70	0.62	0.51	0.58	0.30	-0.29	-0.39	-0.12	0.43	0.32			
LOI	0.94	0.20	0.74	0.73	0.22	-0.10	-0.77	-0.84	-0.62	0.62	0.57	0.43	0.64	-0.72	-0.82	0.24	0.58	0.14	0.72		

Sm: smectite; Mi+Ill: mica+illite; Kln+Hly: kaolinite+halloysite; Qtz: quartz; Kfs: K-feldspar; Pl: plagioclase; LOI: loss on ignition.

Table VII - Comparison between the results of quantitative mineral analyses of the three most interesting kaolin occurrences from Rio de Janeiro, two giant sedimentary kaolin deposits at the North Brazilian region, and the Campo Alegre kaolin deposit in Santa Catarina, Brazil.

[Tabela VII - Comparação entre resultados de análises mineralógicas quantitativas das três mais interessantes ocorrências de caulim do Rio de Janeiro, dois depósitos gigantes de caulim da região Norte do Brasil e depósito de Campo Alegre em Santa Catarina, Brasil.]

Mineralogy	Sedimentary deposits [28]		Campo Alegre [27]			This study		
	Capim River	Jari River	Ox1	Inc2a	Ce2m	RB-4	RB-6	RB-7
Mica+illite	0.0	0.0	6.4	20.9	48.0	1.5	22.9	41.4
Kaolinite+halloysite	100.0	100.0	35.0	65.8	44.3	34.9	23.9	33.3
Gibbsite	0.0	0.0	1.5	0.0	0.0	0.0	0.0	0.0
Quartz	0.0	0.0	4.5	13.2	7.7	27.1	36.4	25.4
K-feldspar	0.0	0.0	52.5	0.0	0.0	36.6	16.8	0.0
Sum	100.0	100.0	99.9	99.9	100.0	100.1	100.0	100.1

or halloysite observed in the kaolin occurrences from Rio de Janeiro are close to those found in the market. However, reserve estimations should be made to evaluate the real economic importance of these deposits. Despite the economic contents of kaolinite and/or halloysite observed in some of the kaolin occurrences from Rio de Janeiro, information about the

size and volume of deposits would provide fundamental data on the importance of these possible deposits.

CONCLUSIONS

The highest kaolinite and/or halloysite content was found

in the RB-4 pegmatite body, which contained kaolinite mixed with tubular halloysite at a concentration of 34.9%, in which kaolinite and halloysite represented values close to 88% in the clay mineral assemblages. The 2nd greatest kaolinite content was found in the RB-7 pegmatite, with 33.3%, representing only 26% of the clay mineral assemblage, with illite as its main component with 74%. The 3rd highest was found in the RB-6 pegmatite, in which kaolinite occurred alone with the content of 23.9%, which accounted for 31% of the clay mineral assemblage. The other pegmatites presented kaolinite and/or halloysite contents ranging from 0 to 18.5%. The samples located in the saprolite zone had the highest kaolinite and/or halloysite contents, following what was observed in the samples RB-2A, RB-4, RB-5, RB-6, and RB-7 (all from Niterói-Rio Bonito area, Brazil). Kaolinite and/or halloysite were generated by weathering processes, in which plagioclase was the most important mineral generator, while K-feldspar and mica were not present in the processes. The market involving industrial ores is more sensitive to economics than traditional ores such as iron and gold. This type of segment is extremely dependent on several economic factors such as current demand, distance from the processing industries, transportation, among others. The economic players must know the available deposits or occurrences of kaolin in Rio de Janeiro, which could lead to new prospects in the future. Furthermore, it is suggested to estimate the reserves of the studied bodies to better evaluate their importance.

ACKNOWLEDGMENTS

We would like to thank the Center for Mineral Technology (CETEM/MCTIC), Federal University of Rio de Janeiro (UFRJ/MEC), the National Council for Scientific and Technological Development (CNPq/MCTIC) for the scholarship (grant number: 131195/2019-0), Federal Rural University of Rio de Janeiro (UFRRJ/MEC), and the Rio de Janeiro State Research Support Foundation (FAPERJ/SCT-RJ).

REFERENCES

- [1] H.H. Murray, in “Applied clay mineralogy”, **1**, Elsevier, Amsterdam (2007) 85.
- [2] H.H. Murray, *Int. J. Miner. Process.* **7** (1980) 263.
- [3] G.J. Churchman, P. Pasbakhsh, S. Hillier, *Clay Miner.* **51**, 3 (2016) 303.
- [4] P. Pasbakhsh, G.J. Churchman, J.L. Keeling, *Appl. Clay Sci.* **74**, 1 (2013) 47.
- [5] V. Vergaro, E. Abdullayev, Y.M. Lvov, A. Zeitoun, R. Cingolani, R. Rinaldi, S. Leporatti, *Biomacromolecules* **11**, 3 (2010) 820.
- [6] B. Guo, Q. Zou, Y. Lei, D. Jia, *Polym. J.* **41** (2009) 835.
- [7] D.G. Shchukin, S.V. Lamaka, K.A. Yasakau, M.L. Zheludkevich, M.G.S. Ferreira, H. Möhwald, *J. Phys. Chem.* **112**, 4 (2008) 958.
- [8] M.S. Prasad, K.J. Reid, H.H. Murray, *Appl. Clay Sci.* **6** (1991) 87.
- [9] R. Gill, *Igneous rocks and processes: a practical guide*, Wiley-Blackwell, Oxford (2010) 375.
- [10] W.D. Johnston Jr, *Geol. Soc. Am. Bull.* **56**, 11 (1945) 1015.
- [11] K.M. Scoot, C.F. Pain (Eds.), “Regolith science”, CSRI Publ., Oxford (2009) 106.
- [12] H.G. Dill, R. Dohrmann, S. Kaufhold, S. Balaban, *Ore Geol. Rev.* **69** (2015) 33.
- [13] J.M. Parker III, “Residual kaolin deposits of the Spruce Pine District, North Carolina”, Techn. Report, North Carolina Dept. Conserv. Devel., USA (1946).
- [14] G.E. Ekosse, *Appl. Clay Sci.* **50** (2010) 212.
- [15] H.M. Fentaw, T. Mengistu, *Appl. Clay Sci.* **13** (1998) 149.
- [16] M.A. Saddiqui, Z. Ahmed, *J. Sci. Eng.* **30** (2005) 195.
- [17] ANM, “Sumário mineral”, DNPM/MME, Brazil (2019) 78.
- [18] D.J. Sousa, A.F.D.C. Varajão, J. Yvon, G.M. Da Costa, *Clay Miner.* **42** (2007) 69.
- [19] C.R. Montes, A.J. Melfi, A. Carvalho, A.C. Vieira-Coelho, M.L. Formoso, *Clays Clay Miner.* **50**, 4 (2002) 494.
- [20] V.M.J. Salgado Campos, L.C. Bertolino, L.C.S. Nascimento, J.Y.P. Leite, V.S. Brandão, O.C. Alves, J. Tolentino Jr., *Clay Miner.* **54**, 3 (2019) 283.
- [21] V.M.J.S. Campos, L.C. Bertolino, O.C. Alves, *Cerâmica* **63**, 367 (2017) 369.
- [22] E.P. Scorza, “Província pegmatítica da Borborema”, Boletim 112, DNPM-DGM/MME, Rio Janeiro, Brazil (1944) 58.
- [23] L.C. Bertolino, D.M.C. Rodrigues, C.L. Roland, O.C. Alves, E. Santos Filho, *Anu. Inst. Geociên. UFRJ* **35**, 2 (2012) 65.
- [24] Y.S. Visconti, N.B.F. Nicot, *Cerâmica* **2**, 6 (1956) 59.
- [25] I.R. Wilson, H. Souza Santos, P. Souza Santos, *Cerâmica* **44**, 287-288 (1998) 118.
- [26] P. Souza Santos, S. Perche Toledo, H. Souza Santos, *Cerâm. Ind.* **14**, 1 (2009) 14.
- [27] M.T.G. De Oliveira, S.M.A. Furtado, M.L.L. Formoso, R.A. Eggleton, N. Dani, *An. Acad. Bras. Ciênc.* **79**, 4 (2007) 665.
- [28] I.R. Wilson, H. Souza Santos, P. Souza Santos, *Clay Miner.* **41**, 3 (2006) 697.
- [29] Y.S. Visconti, N.B.F. Nicot, *Cerâmica* **3**, 10 (1957) 72.
- [30] P. Souza Santos, H. Souza Santos, A.C. Moniz, *Cerâmica* **8** (1962) 2.
- [31] P. Souza Santos, A.C. Pimentel, *Cerâmica* **17**, 67 (1971) 258.
- [32] S.O. Menezes, “Principais pegmatitos do estado do Rio de Janeiro: principais depósitos minerais do Brasil”, v.4b, DNPM/CPRM, Brasília (1997) 405.
- [33] S.O. Menezes, “Catálogo dos principais pegmatitos do estado do Rio de Janeiro”, Niterói, DRM-RJ (1982).
- [34] M. Heilbron, L.G. Eirado, J. Almeida, “Mapa geológico e de recursos minerais do estado do Rio de Janeiro”, CPRM, Belo Horizonte (2016).
- [35] Int. Centre Diffract. Data, PDF4+ (ICDD), Newton

Square (2012).

[36] G.W. Brindley, G. Brown, “Crystal structures of clay minerals and their X-ray identification”, *Miner. Soc. Monogr.* **5**, London (1980) 411.

[37] D.M. Moore, R.C. Reynolds, *X-ray diffraction and the identification and analysis of clay minerals*, 2nd ed., Oxford Un. Press, Oxford (1997).

[38] P.E. Biscaye, *Geol. Soc. Am. Bull.* **76**, 7 (1965) 803.

[39] H.W. Nesbitt, G.M. Young, *Nature* **299**, 5885 (1982)

715.

[40] H.C. Starkey, P.D. Blackmon, P.L. Hauff, “The routine mineralogical analysis of clay-bearing samples”, *U.S. Geol. Survey Bull.* 1563, US Gov. Print. Office, Washington (1984) plate 1.

[41] L. Robb, *Introduction to ore-forming processes*, Blackwell Publ., Oxford (2005).

(*Rec.* 20/03/2020, *Rev.* 26/05/2020, 22/06/2020, *Ac.* 29/06/2020)

